Retention During Freezing of Raindrops, Part II: Investigation of Ambient Organics from Beijing Urban Aerosol Samples

Jackson Seymore*[1], Martanda Gautam[1], Miklós Szakáll[1], Alexander Theis[2], Thorsten Hoffmann[2], Jialiang Ma[3], Lingli Zhou[4], Alexander L. Vogel[3]

[1] Institute for Atmospheric Physics, Johannes Gutenberg University, Mainz, Germany
[2] Particle Chemistry Department, Max Planck Institute for Chemistry, Mainz, Germany
[3] Institute for Atmospheric and Environmental Sciences, Goethe University Frankfurt, Germany
[4] South China Institute of Environmental Sciences, Ministry of Ecology and Environment, Guangzhou, P.R. China
*Corresponding author: seymorej@uni-mainz.de

Keywords: retention, dissolved organic matter, DOM, Orbitrap MS, secondary organic aerosol, SOA, convective clouds, acoustic levitator

Abstract

The freezing of hydrometeors causes certain water-soluble organic compounds dissolved in the supercooled cloud droplets to be released into the gas phase. This may lead to the vertical redistribution of substances that become available for atmospheric processes in the upper troposphere such as new particle formation or ozone formation. Drop freezing experiments were performed on the Mainz Acoustic Levitator (M-AL) using aqueous extracts of ambient samples of Beijing urban aerosol. The retention coefficients of over 450 compounds were determined. Most nitroaromatics and organosulfates were fully retained along with the aliphatic amines (AA) and higher-order amines and amides while the observed sulfides, lipids, aromatic hydrocarbons, and long chain compounds are among the most unretained and incidentally the fewest species present. The findings here also indicate that N- and S- containing compounds, primarily nitro and sulfate components of secondary organic aerosols (SOA) anthropogenically related to NO_x and SO_2 chemistry, have enhanced retention likely due to their increased polarity. An insignificant positive correlation between polarity and freezing retention along with a significant negative correlation with vapor pressure and freezing retention was observed. No sigmoidal relationship with effective Henry's law constant was observed. This differs from the parameterizations of

riming retention presented in current literature, which is justified by the lower surface-to-volume ratio of the large drop size investigated. This study greatly expands on the available experimental measurements of retention by investigating hundreds of compounds in complex chemical conditions more similar to the atmosphere than the previous literature studies.

1 Introduction

Atmospheric organic matter (OM) plays a critical role in climate regulation directly through radiation scattering and indirectly through cloud condensation nucleation which impacts Earth's energy balance through radiative forcing (Fofie et al., 2018; Liu et al., 2018). These effects are controlled by factors such as their optical properties, size, and the hygroscopicity (Dusek et al., 2006; Sun et al., 2021), which can change based on the proportions of primary organic aerosols (POA)—directly emitted aerosols—and secondary organic aerosols (SOA)—aerosols formed from the oxidation products of volatile organic compounds (VOC)—as well as inorganic constituents (Hallquist et al., 2009; Liu et al., 2021; Riva et al., 2019). Convective systems have been suggested to support new particle formation (NPF) in the outflow region by reducing existing particle concentrations, facilitating cold temperatures, and transporting reactive gases into regions with high actinic fluxes (Clarke et al., 1998; Zheng et al., 2021)

Nucleation-mode particles—with sizes in the lower tens of nm—have consistently been observed in concentrations of up to 10^4 cm^{-3} from aircraft in the upper troposphere (Andreae et al., 2018; Andrés Casquero-Vera et al., 2020; Clarke et al., 1999; Heitto et al., 2024; Weigel et al., 2011; Williamson et al., 2019). These measurements significantly exceed the corresponding concentrations in the planetary boundary layer and indicate that the main source of such ultra-fine particles in the upper troposphere is in situ NPF rather than their direct transport from the boundary layer (Bardakov et al., 2021). The traditional explanation for this phenomenon has been that the reduction of existing aerosol particles in deep convective clouds eliminates removal processes for small particles and condensable vapors, supporting

NPF (Clarke et al., 1998). However, Williamson et al. (2019) also showed that even without these conditions, such as in tropical convection, these newly formed particles can still be found. They then argue that most models underestimate available organic matter at high altitudes and as a result predict less NPF in these regions. If this NPF is the result of an overlooked mechanism of organic matter transport, it is then critical to elucidate this mechanism for NPF precursors so to constrain uncertainty around the influence of high altitude NPF from convective outflows (Bardakov et al., 2021).

Publications by Borchers et al. (2024) and Jost et al., (2017) have demonstrated a potential mechanism for organic matter transport in mixed-phase clouds. They describe how organic compounds that are exchanged between the gas and aqueous phase in cloud droplets can either be trapped in the ice phase during freezing—washing them out by precipitation—or return to the gas phase by volatilization. This revolatilization caused by the freezing process leads to a vertical redistribution and has the potential to explain the occurrence of organic matter at high altitudes in regions with deep convection. Alternatively, earlier publications by Pruppacher and Klett (2010) and Snider and Huang (1998) have suggested that complete sublimation of ice particles can also transport 'retained' compounds trapped in the ice phase and release them at high altitudes.

In convective clouds the main formation pathway of precipitation-size ice particles is riming, i.e. the freezing of supercooled µm-sized cloud droplets on the surface of a mm-sized ice particle. Thus, riming retention is an important process for the vertical redistribution of water-soluble organic compounds (WSOC). Convective clouds with warm bases favor the formation of mm-sized drops by collision-coalescence (Lamb and Verlinde, 2011), which subsequently can be uplifted in the updraft to regions with temperatures below 0°C. Once beyond the freezing level they can freeze and thereby release dissolved matter into the gas phase. This identifies freezing retention of mm-sized drops as a potential contributor to the vertical redistribution of WSOCs and was experimentally investigated in the present study.

75   The proportion of a substance that remains in the ice during this phase change is described by the

retention coefficient R, which indicates the percentage of the trapped substance with a value between 0

and 1 (Bela et al., 2018; Iribarne and Pyshnov, 1990; Snider et al., 1992; Stuart and Jacobson, 2004). A

species' retention is influenced by its chemical properties, such as its dimensionless effective Henry's law

solubility constant (H*), as well as the physical properties such as temperature, liquid water content,

80   droplet size, and ventilation. Substances with a small H* are more likely to return to the gas phase during

riming, which results in a lower retention coefficient. Additionally, these external and physical conditions

of the droplet disproportionally influence the retention for these small H* substances (Jost et al., 2017;

Stuart and Jacobson, 2003, 2004)

Current experimental studies to determine retention coefficients for atmospheric constituents and

85   relevant SOA precursors have focused on inorganic species, small organics, or single component mixtures

with significantly higher than natural concentrations. Additionally, current studies have only examined

retention for cloud droplet sizes rather than raindrop sizes. The few studies that look at complex mixtures

are limited to compounds of similar families and only a handful of species (Borchers et al., 2024).

Naturally occurring atmospheric constituents that are observed in rainwater are present as complex

90   mixtures of potentially thousands of species (Seymore et al., 2023). To get closer to observing the

retention of compounds in their natural conditions, this study presents measurements of retention

coefficients for a real, complex mixture of WSOC extracted from filter samples taken in an urban

environment.

2 Methods

2.1 Sampling Location and Method

A high-volume sampler (HiVol) was run with quartz fiber TSP filters over three nights between March 3 and 5, 2022 in Beijing, China (40.0426° N, 116.4197° E) for an approximate sample volume of 550 m^3 between the hours of 21:00 to 9:00. These filters were sealed in aluminum foil and stored at −20⁰C until analysis. Aqueous extracts of these filters were prepared by taking 1/4 of each filter, combining them (in total 3/4 of a 203 x 254 mm filter area) in 30 ml Milli-Q water, and then extracting with an orbital shaker for 15 min. Multiple filters were used to produce the filter extract sample in order to ensure adequate concentration and uniform background signal across multiple measurements. This also controls for potential differences in matrix effects from different filter compositions. The same extraction was performed for a blank sample; a total 3/4 of unsampled filter area was extracted in 30 ml Milli-Q water for 15 min. These extracts were filtered through a 0.2 µm PTFE filter. 10 ml of the prepared extract was reserved for Ultra-High Performance Liquid Chromatography High-Resolution Orbitrap Mass Spectrometry (UHPLC-HRMS) analysis and stored at 3 ⁰C while the remaining 20 ml was sent to Institute for Atmospheric Physics at the Johannes Gutenberg University of Mainz, Germany for freezing experiments.

2.2 Mainz Acoustic Levitator (M-AL)

Freezing experiments were performed in an acoustic levitator (APOS BA 10, tec5 GmbH). This allows contact-free single-drop levitation maintained by a standing ultrasonic wave. This setup and its relevant physical influences are described in detail by Diehl et al., (2014), Szakáll et al., (2021), and in part 1 of this publication series by Gautam et al. (2025). For the freezing experiment, the M-AL is placed inside a walk-in cold room where the ambient temperature was set to −15⁰C. The M-AL is surrounded by a protective acrylic housing to prevent any disturbance from air motion which may cause unsteady

temperature conditions, unstable levitation, or carry unwanted ice-nucleating particles onto the drop

120   surface. Air temperature in the M-AL was measured by a PT100 sensor and an infrared thermometer (KT 19.82 II, Heitronics) was used to monitor drop surface temperature.

The aqueous filter extract was injected with a syringe into the M-AL node to form a single free-floating drop with a diameter of 2 ± 0.1 mm. The drop was allowed to freeze without the introduction of artificial freezing nucleator. Freezing time was approximately 90 seconds on average but not longer than 3

125   min. Once the drop was fully frozen, it was removed from the M-AL and stored in a polytetrafluoroethylene (PTFE) vial at $-20ºC$ until analysis. Enough drops to reach the minimum viable sample volume for analysis, 50 µl, were collected to produce a single sample (approximately 12 drops). 30 drops were produced in total, which allowed for two full samples to be used for UHPLC-HRMS analysis. The blank filter extract was also used in the freezing experiment to produce two more travel

130   blank samples for comparative analysis and background subtraction.

2.3 UHPLC-HRMS analysis

In addition to the M-AL frozen extract and the travel blanks, 100 µl of the reserved extract and Milli-Q solvent was analyzed by UHPLC-HRMS. Chromatographic separation was performed (Vanquish

135   Flex, Thermo Fisher Scientific Inc.) on a reversed phase column (Cortecs Solid Core T3, 2.7 µm, 150 × 3 mm, with the corresponding VanGuard Cartridge, Waters Corp.). Samples were ionized in negative and positive mode using a heated electrospray ionization source (HESI-II Probe, Thermo Fisher Scientific Inc.) and then detected with a high-resolution hybrid quadrupole-Orbitrap mass spectrometer (Q Exactive Focus, Thermo Fisher Scientific Inc.). The chromatographic settings and gradient are as follows: LC

140   solvent A: ultrapure water with 0.1% formic acid; LC solvent B: methanol with 0.1% formic acid; Flow rate 400 µl min^{-1}; pre-column heater and post-column cooler 40 °C; Gradient: 0 min 1% B; 1 min 1% B; 15 min 99% B; 16.5 min 99% B; 17.5 min 1% B; 20 min 1% B. The MS settings were at fullMS scan

(*m/z* 50-750; resolution 70k) along with data-dependent MS2 in discovery mode (resolution at 17.5k) for acquiring fragmentation spectra of the largest peaks.

145

2.4 Non-targeted Analysis and Property Estimation

Compound identification confidence is communicated here using the convention described in Schymanski et al., (2014). The raw UHPLC-HRMS files were processed on Compound Discoverer 3.3 (Thermo Fisher Scientific). This software aligned chromatographic peaks of interest with a maximum shift of 0.1 min in retention time and a mass tolerance of ±2 ppm. Mass traces with retention times less than 1.8 min were excluded as they are not considered to be chromatographically separated. Ions were detected if the peak intensity was at least 5×10^5 counts for $[M-H]^-$ for negative mode or $[M+H]^+$ and $[M+Na]^+$ for positive mode. In addition to the mass-to-charge ratio of the detected ion, at least one corresponding isotopologue had to be measured. The tolerance between the measured and calculated intensity of the isotopologue was less than 30 %. These unknown compounds were then grouped with a retention time tolerance of 0.1 min to produce a merged MS feature and those of them with a sample-to-blank ratio smaller than 5 were marked as background and removed from the dataset. Any compounds that did not appear in the reserved sample of filter extract were also removed from the dataset. A peak quality score was given on a scale of 0 to 10—with 10 being a perfect chromatographic peak—for each mass trace based on its peak shape qualities, e.g. peak jaggedness, modality. For all mass traces with a peak quality higher than 6 in all samples, a predicted composition for each mass trace was calculated within ±2 ppm with the allowed elements of carbon (C), hydrogen (H), nitrogen (N), oxygen (O), and sulfur (S). Compounds were grouped together as CHO, CHNO, CHOS, and CHNOS. It is important to note that phosphorus (P) containing species were not considered for this study. All level 5 (L5) through level 1 (L1) compounds including any mass traces that did not fit a predicted composition within ±2 ppm were used for calculating retention coefficients using their integrated MS signals. Level 4 (L4) through L1 compounds with determined compositions were used for Van Krevelen and Kroll analysis to highlight the

validity of the dataset as a real, complex mixture of urban-influenced WSOC. To aid the visualization of MS data, a Van Krevelen diagram cross-plots the H:C ratio as a function of the O:C ratio while a Kroll

170   diagram cross-plots the estimated average carbon oxidation state as a function of the number of carbon atoms. An estimated vapor pressure at 298 K was then calculated for the elemental composition based on the parameterization by Li et al. (2016).

The predicted compound list was then matched against the mzCloud database (HighChem LLC, 2013-2021) for comparing MS^2 spectra. If a compound had at least one positive match with the predicted

175   compound in the database as well as a peak quality score above 8 in the reserved extract, this level 3 (L3) or stronger candidate was selected to be used for calculating its effective Henry's law constant (K_H, mol Pa^{-1} m^{-3}). This was predicted using the HENRYWIN™ model as part of the EPI Suite™ package which provides the values at 298 K (US EPA, n.d.). If the EPI Suite™ was able to find an experimental value based on a CAS lookup match, those values were used over the model prediction. This is only applicable

180   to the minority of identified species. The effective Henry's law solubility was converted to a dimensionless effective Henry's law constant (H*) using the equation:

$$H^* = K_H * \bar{R}T \qquad (1)$$

Where $\bar{R}$ is the ideal gas constant (8.3144626 m^3 Pa K^{-1} mol^{-1}) and T is temperature (K). This conversion allows for a dimensionless comparison and considers dissociation and hydration effects. This calculation,

185   however, requires structural information about a compound. As a result, performing this calculation on a L3 tentative structural candidate can be specious or misleading. Regardless, H* for structural isomers using HENRYWIN™ typically differs less than 3 orders of magnitude with an overall average of approximately 1.5. This accuracy is sufficient for this analysis (Isaacman-Vanwertz and Aumont, 2021).

2.3 Retention Calculation and Tracer Corrections

The signals of species that also appeared in the travel blanks were first subtracted from the M-AL samples to remove their ambient signal but remained in the dataset as they exceeded the sample-to-blank ratio of 5 and could not be considered background. A naturally occurring tracer was selected from the dataset for both positive and negative mode to correct for any dilution, evaporation, and desorption that may occur. To be an ideal tracer, the compound should be fully retained during freezing and have an adequate MS signal. For this work, the peak quality was required to be higher than 8 in the reserved extract and for there to be a positive database match for the predicted composition. For negative mode, this tracer was 4-Nitrophenol ($C_6H_5NO_3$, 139.0269 m/z, 9.7 min, L3). This was chosen as previous experiments by Borchers et al., (2024) have identified this compound to have a retention coefficient of 1.01 ± 0.07 during riming experiments, where desorption and evaporation effects are likely to be more influential than in the present experiment due to enhanced ventilation and much smaller droplet size. For positive mode, xylitol ($C_5H_{12}O_5$, 152.0685 m/z, 1.6 min, L3) was selected as the tracer as its H* has been determined to be higher than 10^8 (Compernolle and Müller, 2014), which according to Borchers et al., (2024) and Jost et al., (2017) indicate its retention coefficient can be safely assumed to be 1, even under the higher exchange conditions of wind tunnel experiments. Regardless of the accuracy of the L3-assigned structure, these tracers represent species with retentions very close to 1 that allow for a reference to that value to compare between samples and make corrections for non-freezing mass exchange.

The equation for calculating the retention coefficient is adopted from Borchers et al., (2024) and Jost et al., (2017) and used here as

$$R = \frac{S_{substance}^{sample} / S_{substance}^{RES}}{S_{tracer}^{sample} / S_{tracer}^{RES}} \tag{2}$$

where the numerator describes the ratio between the peak area of the substance of interest in the ice sample ($S_{substance}^{sample}$) and in the reserved extract sample ($S_{substance}^{RES}$). The denominator describes the same

ratio but for the tracer ($S_{\text{tracer}}^{\text{sample}}$ / $S_{\text{tracer}}^{\text{RES}}$). Since no dilution effects are involved in the measurement and all samples are measured in the same aqueous matrix, signal ratios can be compared directly without a calibration curve, provided that detector response is linear within the given range of measurement. Given that ions below the threshold intensity of linearity were excluded from measurement, dynamic mass calibration of the HRMS was performed prior to measurement, and that HRMS instruments of this generation show linear dynamic ranges of at least five orders of magnitude (Kaufmann and Walker, 2017), it is reasonable to assume linearity over the measurement range. As ventilation and evaporation effects are quite low in the M-AL (Szakáll et al., 2021), their effects are compensated for by the tracer. Compensating for desorption effects is more complex. As desorption is thought to be driven mainly by linear diffusion and thus enhanced by increased ventilation, species with higher than ambient concentrations as well as species with higher vapor pressures are thought to be disproportionally influenced. However, since the M-AL has little ventilation to enhance desorption, HiVol filter sampling already bias against high vapor pressure species (Bidleman et al., 2020), and ambient filter sampling is closer to ambient concentrations relative to previously simulated single component mixtures, desorption effects are only compensated for by the tracer and nonuniform desorption effects are considered negligible.

Further data analysis was performed with MATLAB ver. R2023a. Distribution modeling was performed using the Distribution Fitter from the Statistics and Machine Learning Toolbox 12.5, based on the Stable Distribution and t Location Scale Distribution models provided in *Univariate Stable Distributions* (2020) and *Univariate Continuous Distributions* (2015) (Nolan, 2020; Yee, 2015).

3 Results and Discussion

3.1 Dataset Description

In the negative mode, from over 2800 MS features measured, 548 significant, non-background detected compounds were found. 208 met the peak quality constraints and were then used for analysis.

196 compounds (94%) had successfully assigned compositions and 77 were then selected for additional property calculations.

In the positive mode, 342 significant, non-background detected compounds were found from over 1800 features. 250 met the peak quality constraints and were then used for analysis. 218 of those compounds (87%) had successfully assigned compositions. 84 were then selected for additional property calculations. Comparatively fewer compounds were assigned compositions in the positive mode as phosphorous containing species were not considered. Phosphorous containing species can represent almost a third of positively ionizable species in rainwater WSOC (Seymore et al., 2023) so these species likely make up a significant portion of species variety that is not considered.
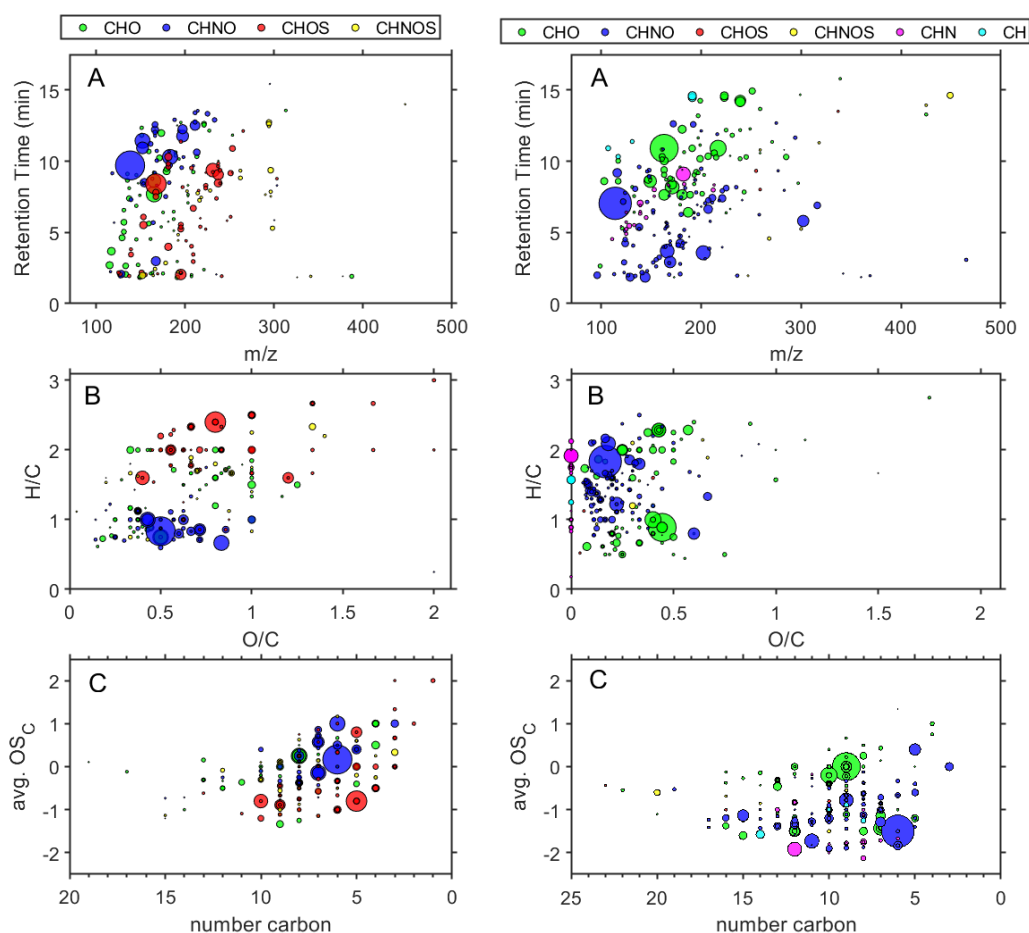
Figure 1. (A) Scatter plot of HPLC Retention time (min) vs m/z ratio; (B) van Krevelen diagram of O/C ratio vs H/C ratio; (C) Kroll diagram of number of C atoms against the average oxidation state of C; Left panels are for negative ionization mode (−)HESI, right panels are positive ionization mode (+)HESI. Area of the marker indicates relative intensity in the reserved extract while color denotes compositional class of the assigned compound: Green for CHO, blue for CHNO, red for CHOS, yellow for CHNOS, magenta for CHN, cyan for CH.

Figure 1 illustrates that the dataset is indicative of a typical urban influenced WSOC profile of a dilute sample. In the negative mode, the most significant signals are several nitrophenols and nitroaromatics; notably $C_6H_5NO_3$ (139 m/z, 9.7 min, L3) and $C_6H_4N_2O_5$ (184 m/z, 10.3 min, L3) are tentatively identified as either 4-nitrophenol and 2,4-dinitrophenol respectively. These nitrophenols ionize efficiently in (−)HESI which explains in part their prominence in Figure 1.B where they cluster around 0.6-0.9 H/C and are indications of biomass and fossil fuel burning emissions (Taneda et al., 2004). The prominent CHOS compounds in the negative mode are alkylorganosulfates, notably $C_5H_{12}O_4S$ (168 m/z, 8.4 min, L3) and $C_8H_{18}O_4S$ (210 m/z, 12.9 min, L3), which are typical markers of secondary processed automobile and shipping traffic OM (Blair et al., 2017; Qi et al., 2021). These can most easily be seen in Figure 1.B above 2 H/C. Some of the other notable CHOS compounds below 2 H/C are terpene-derived organosulfates in addition to compounds such as camphorsulfonic acid ($C_{10}H_{16}O_4S$, 232 m/z, 9.4 min, L2), which also demonstrate secondary processing with sulfate aerosols (Iinuma et al., 2007; Surratt et al., 2007).

The most significant positive mode signals in Figure 1 come from caprolactam ($C_6H_{11}NO$, 114 m/z, 7.0 min, L2) and several coumarin derivatives ($C_9H_6O_2$, 146 m/z 7.4 min, L2; $C_9H_8O_4$, 162 m/z, 10.9 min, L3; $C_9H_8O_3$, 164 m/z, 8.7 min, L3; $C_{10}H_8O_4$, 192 m/z, 9.0 min, L3). Caprolactam is a cyclic amide and indicative of industrial emission influence as it is primarily used for manufacturing synthetic fibers but also used in numerous other manufacturing activities. Caprolactam is a monitored compound on the

hazardous air pollutants list by the United States Environmental Protection Agency (U. S. Environmental Protection Agency, n.d.). Coumarin species are known brown carbon components and have biomass burning sources as well as potential secondary pathways (Xing et al., 2023).

275   The several other prominent CHNO compounds are mostly amines, e.g. $C_{11}H_{23}NO_2$ (201 *m/z*, 3.6 min, L3), $C_9H_{11}NO_2$ (165 *m/z*, 3.7 min, L3), DL-Stachydrine ($C_7H_{13}NO_2$, 143 *m/z*, 1.8 min, L2), etc. This is consistent with known amine-nitrate aerosol formation during winter months where there are sources of amine salts and semi-volatile organic amine compounds, particularly in areas with high agricultural and combustion emissions (Price et al., 2016). The other prominent CHNO compounds are tentatively

280   identified as amides such as $C_{12}H_{18}N_2O$ (206 *m/z*, 6.6 min, L3), $C_{10}H_{14}N_2O$ (178 *m/z*, 4.2 min, L4), $C_3H_4N_4O_2$ (128 *m/z*, 1.8 min, L3), etc; which can either be further secondary products of AA (Price et al., 2014) or the result of anthropogenic emissions (Li et al., 2022; Schollée et al., 2017). These amine and amides tend to have lower retention times and can been seen in the lower cluster in Figure 1.A. The CHO species present are generally either aromatics or aliphatic acids and separate out as so in the van Krevelen

285   diagram in Figure 1.B, with aromatics below 1.5 H/C and acids above such as $C_{12}H_{24}O_3$ (216 *m/z*, 14.2 min, L3) and $C_9H_{10}O_3$ (166 *m/z*, 9.1 min, L3). Very few biogenic CHO species are present as there are very few CHO species within 1.5-1.8 H/C that would indicate humics, ligins, or other raw biomass markers (Qian et al., 2013). This is consistent with the winter season sampling (Ma et al., 2022). Further characterization of the nonaromatic CHO is difficult to generalize, as there are a variety of sugars, ethers,

290   alcohols, and acids that represent various possible biogenic species, terpenoids, and terpene derivatives. For example, xylitol (possibly arabitol) ($C_5H_{12}O_5$, 152 *m/z*, 1.6 min, L3), hexitol ($C_6H_{14}O_6$, 182 *m/z*, 1.6 min, L3), cinnamic acid ($C_9H_8O_2$, 148 *m/z*, 8.7 min, L3), phthalates such as dimethyl phthalate ($C_{10}H_{10}O_4$, 194 *m/z*, 10.9 min, L2) and phthalic acid ($C_8H_6O_4$, 166 *m/z*, 7.6 min, L3), as well as succinic acid ($C_4H_2O_3$, 98 *m/z*, 2.6 min, L3), levoglucosan ($C_6H_{10}O_5$, 162 *m/z* , 4.5 min, L2) and farnesol ($C_{15}H_{26}O$, 222

295   *m/z*, 14.6 min, L3) are all species potentially identified in the dataset.

A few CH and CHN compounds were found only in the positive mode, primarily AA and a couple of aromatic hydrocarbons. Combined, these represent less than 11% of the positive mode compounds. Only one CHS species was identified ($C_{18}H_{12}S$, 260 *m/z*, 10.0 min, L4) but was not used for analysis as it was below peak quality requirements. No CH, CHN, or CHS species were found in the negative mode.

300

3.2 Retention Coefficients

Table 1. Mean and Median Retention Coefficients by Compound Class and Heteroatom Group

	(−)HESI					(+)HESI				
	Mean	**σ**	**Median**	**n**	**n%**	**Mean**	**σ**	**Median**	**n**	**n%**
Total	0.95	0.21	0.96	208	100	0.95	0.53	0.93	250	100
CHO	0.90	0.25	0.91	68	32.7	1.01	0.82	0.90	73	29.2
CHN	-	-	-	-	-	1.07	0.21	1.04	22	8.8
CHNO	0.96	0.08	0.95	46	22.1	0.94	0.21	0.93	108	43.2
CHNOS	0.97	0.23	0.98	26	12.5	1.11	0.34	0.99	7	2.8
CHOS	0.99	0.23	0.98	56	26.9	0.67	0.59	0.99	3	1.2
CH	-	-	-	-	-	0.66	0.55	0.78	5	2.0
O Containing	0.95	0.21	0.96	196	94.2	0.97	0.54	0.92	191	76.4
N Containing	0.96	0.15	0.96	73	35.1	0.97	0.22	0.95	137	54.8
S Containing	0.99	0.23	0.98	83	39.9	0.98	0.44	0.99	10	4.0

305
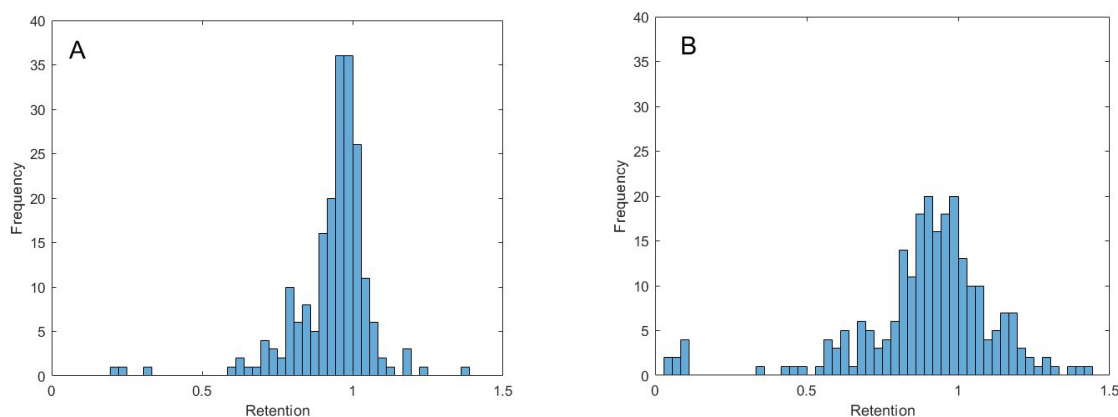
Figure 2. Histograms of Retention Coefficients for all measured L5 and above compounds that met peak quality constraints; (A) (−)HESI, (B) (+)HESI
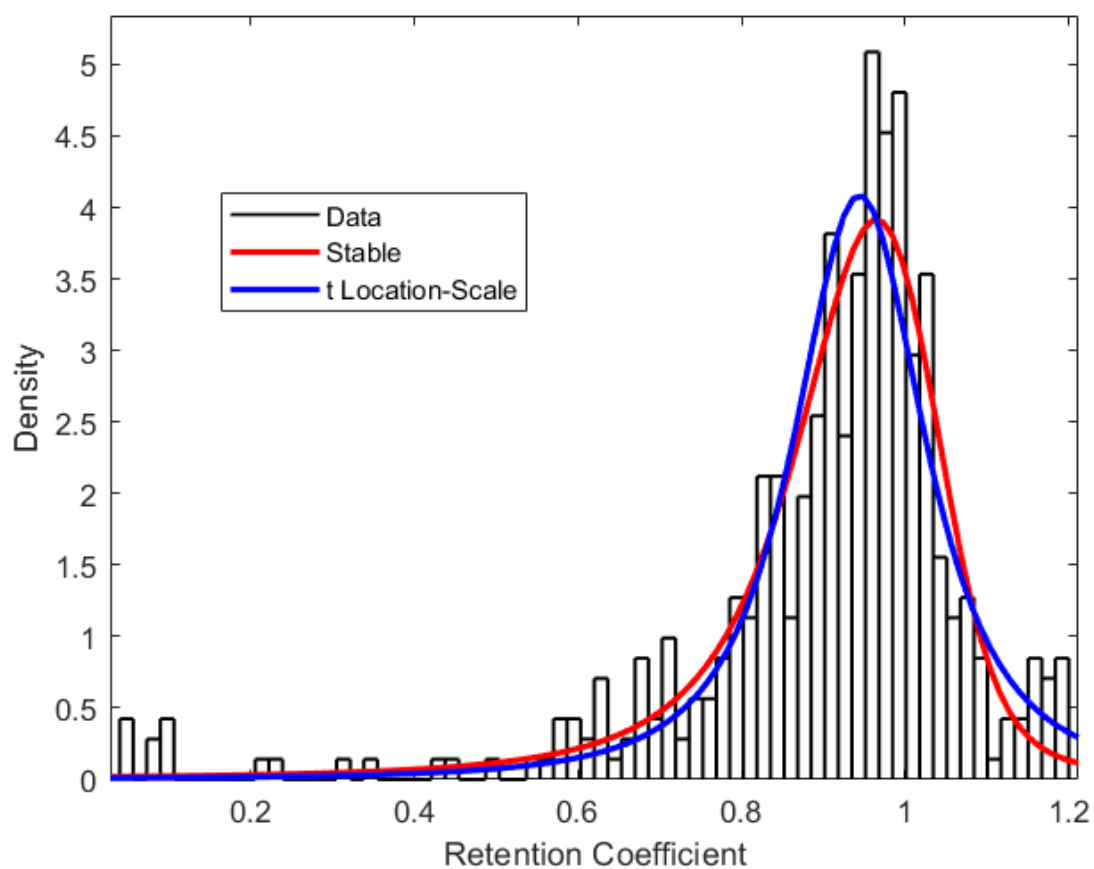
310

Figure 3. Merged Histogram for (−)HESI and (+)HESI of all Retention Coefficients measured fit with Stable and t Location-Scale distribution parameterizations of statistical density.
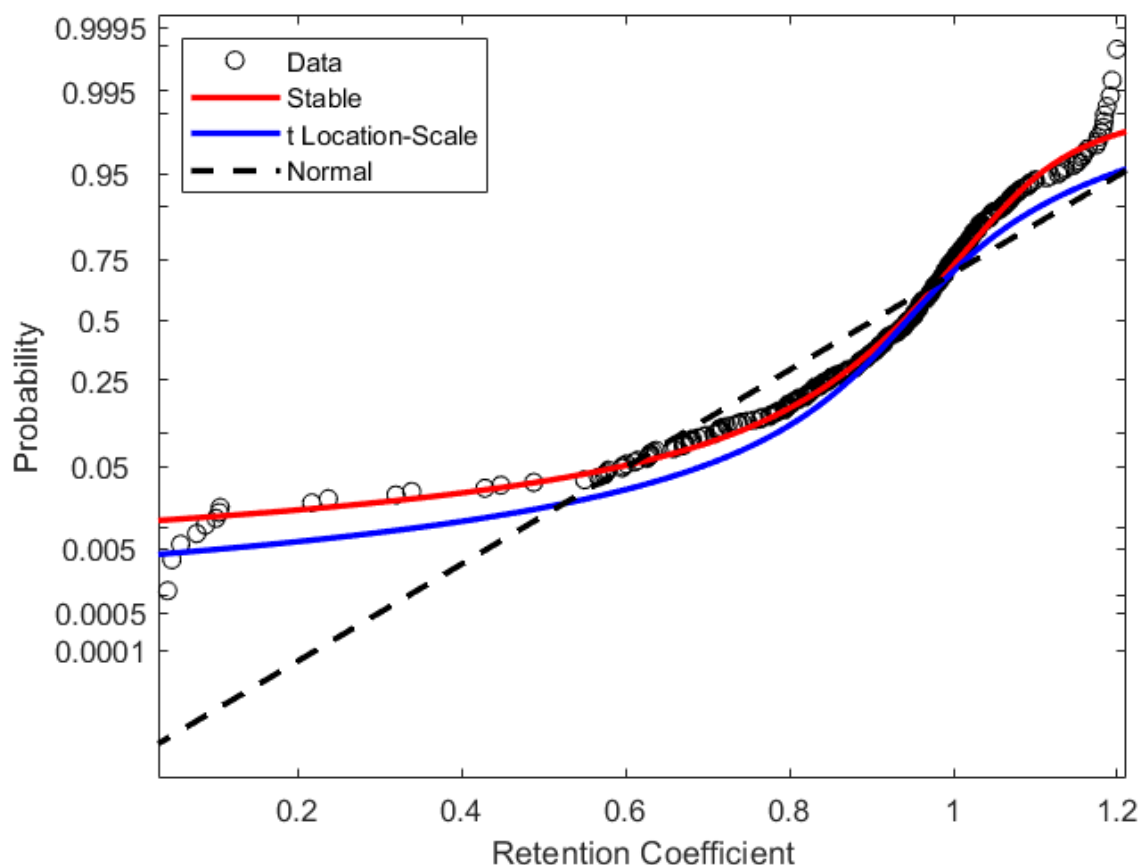
Figure 4. Probability plot of Retention Coefficients with the Stable and t Location-Scale distribution parameterizations and a Normal distribution

The histograms presented in Figure 2 and Figure 3 illustrate the distribution of retention coefficients determined for this dataset. Each histogram shows a peak at 0.96, 0.93, and 0.94 for (−)HESI, (+)HESI, and the full dataset respectively with average retentions all at 0.95 with standard deviations of 0.21 and 0.53 respectively. These values and the values for each compound class are presented in Table 1. Visually the distributions in Figure 2 appear nonnormal, suggesting a true distribution is being measured. Additionally, Figure 4 shows the data deviates strongly from a normal distribution. Both Shapiro-Wilk and Shapiro-Francia tests indicate nonnormality (p-values: 0.4052, 0.3940 (−)HESI; 0.5698, 0.5611 (+)HESI respectively).

325   Combining these distributions and filtering out outliers, the dataset is fitted with two distributions

to model the dataset: Stable and t Location-Scale. The parameters for these fits can be found in the

Supplemental Information as Tables S1 and S2. These distributions are functional estimations of the

statistical density of retention coefficients based on the empirical measurements in this experiment. The

Stable distribution appears to model the data most accurately as the parameter errors are lower than the t

330 Location-Scale and the data points in Figure 4 lie closer to the Stable distribution curve.
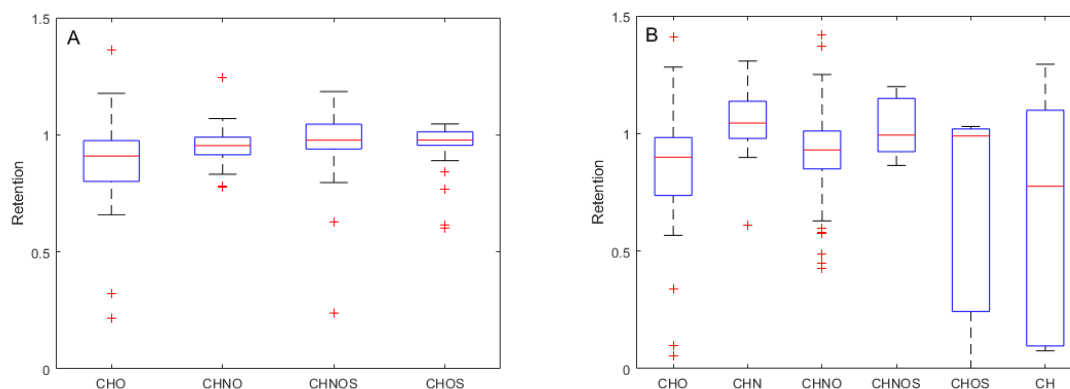
Figure 5. Boxplot of Retention Coefficients by Composition Class; (A) (−)HESI, (B) (+)HESI

335   The means of the composition classes in (−)HESI range between 0.90 and 0.99 with an

unweighted average of 0.95 and a standard deviation between them of 3%. In contrast, the means of the

composition classes in (+)HESI vary more, up to 40%. The deviations and ranges of values are also wider

in (+)HESI, from 0.21 to 0.82 as seen in Table 1. Visually this can be seen in Figure 5. For both

ionizations, CHNOS tends to be the highest retained along with CHN in (+)HESI. These CHNOS

340 compounds have some of the highest molecular masses in the dataset, evident in Figure 1. The CHN

species present are all AA. In (+)HESI, CHNOS, CHOS, and CH represent the smallest portion of the

dataset—less than 6%—and some of the most variably retained species. For CH, this follows with the

variability in hydrocarbon aqueous solubility, however this variability is more likely explained for

345 CHNOS, CHOS as well with the smaller sample set bias. Notably, with lower median retentions in both ionizations, most CHO compounds have lower retentions than CHNO compounds. In (−)HESI, CHNO is mostly nitroaromatics while in (+)HESI, CHNO is mostly amines and amides. CHO represents a more similar distribution of organic acids and terpenoids in both positive and negative mode, with more nonpolar species represented in (+)HESI. The lower retention among CHO may then be based on its distribution of organic acids versus terpenoids. This data suggests that nitrate species and amines/amides

350 have similar retentions. It is known that NOₓ participates in the reversible and irreversible uptake of isoprene to aerosol liquid water and can further react with isoprene to produce a substantial number of organonitrates (El-Sayed et al., 2018; Tsiligiannis et al., 2022). While it's also known that organic nitrogen represents an important fraction of WSOC (Saxena and Hildemann, 1996; Zhang et al., 2002), this data may also indicate that nitrogen chemistry on CHO species enhances their retention in

355 hydrometeors. Other UHRMS studies of rainwater have suggested similar explanations for nitrogen uptake in hydrometeors and rainwater organic nitrogen's high bioavailability (Seymore et al., 2023).
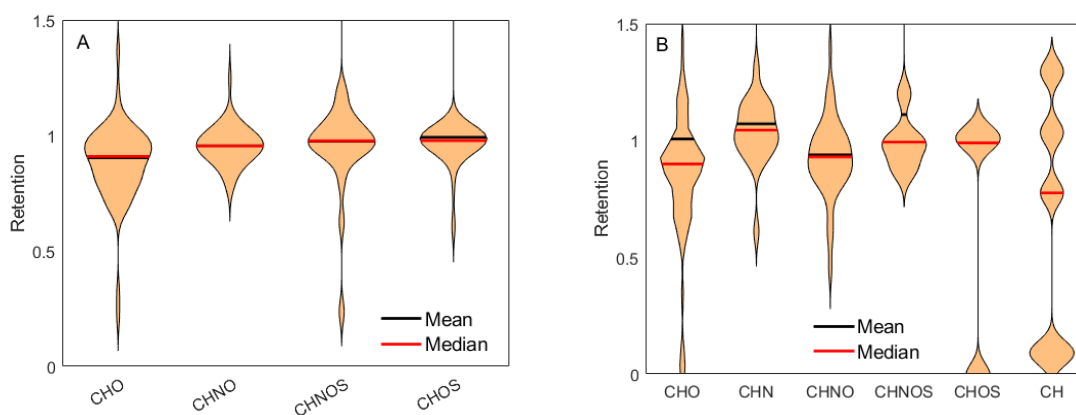
Figure 6. Violin plots of Retention Coefficients by Composition Class; (A) (−)HESI, (B) (+)HESI

360   The distributions of CHNO and CHOS in (−)HESI seen in Figure 6 show a coincidence of the mean and median along with strong symmetry around the mean. This indicates visually that they appear to be normally distributed, suggesting that the true retentions for the whole of these compound classes may be close to 1. Both Shapiro-Wilk and Shapiro-Francia tests indicate normality (p-values: 0.1920, 0.1922) for CHNO but not for CHOS (7.7595×10^{-9}). It therefore would be reasonable to assume a

365   normal distribution for CHNO, but CHOS cannot be rigorously stated as normally distributed. CHO and CHNOS show unique distributions with a significant number of values within $-\sigma$ and below, indicating there are certain CHO species that are not retained during freezing.

        For (+)HESI, the samples sizes for CHNOS, CHOS, and CH are too small to make meaningful descriptions of their distributions. For CHO, CHN, CHNO, the distributions are visually nonnormal and

370   also do not pass any statistical test for normality. The distributions also appear less smooth than their negative mode counterparts, likely a result of previously discussed ionization variability in (+)HESI. Notably, (+)HESI shows a few species with very low retention specifically within the CHO, CHOS, and CH groups. Specifically, these are $C_{14}H_{22}$ (190 *m/z*, 14.5 min, L3), $C_{15}H_{26}O$ (222 *m/z*, 14.6 min, L3), and what appears to be a phenyl-sulfide species ($C_{16}H_{18}OS$, 258 *m/z*, 8.0 min, L4). This is the only identified

375   organosulfide within the dataset. It would be speculative to say that its low retention may indicate that organosulfides as a class are unretained and thus unlikely to appear in the dataset. Its low retention likely has more to do with its low polarity. $C_{14}H_{22}$ and $C_{15}H_{26}O$ as long chain, nonpolar species demonstrate that species with lower aqueous solubilities are also likely to have low retentions.

        Concerning heteroatoms, the distributions and ranges of retentions are quite similar among all groups.

380   Oxygen-containing species appear to have a slightly wider distribution which is mostly weighted by the CHO class. Nitrogen-containing species have a smaller standard deviation than the O or S containing species, indicating fewer species with variable retentions and more fully retained compounds. This further suggests that nitrogen inclusion enhances retention (see also Figure S1).

385   3.3 Correlation of Retention Coefficients with Chemical Properties
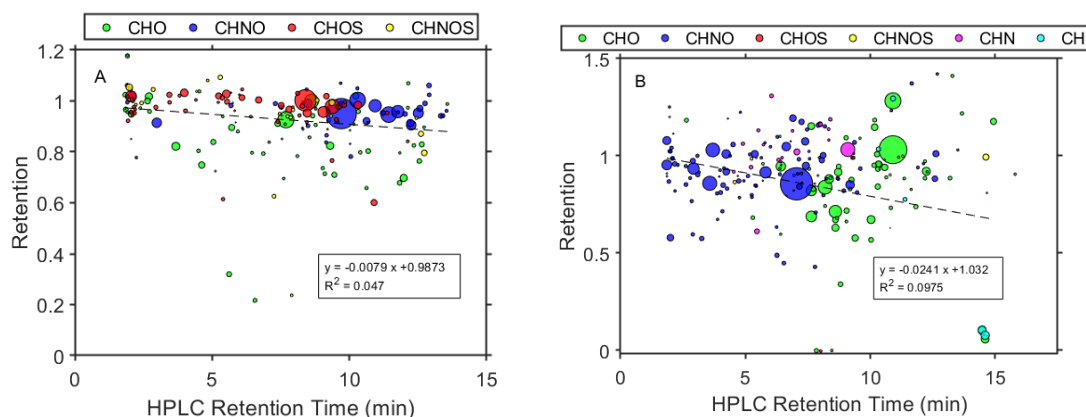
Figure 7. Retention Coefficient as a function of HPLC Retention time; (A) (−)HESI, (B) (+)HESI; Color

390   denotes compositional class of the assigned compound, as used in Fig. 1: Green for CHO, blue for

CHNO, red for CHOS, yellow for CHNOS, magenta for CHN, cyan for CH. Dashed line shows linear fit.

Figures 7 shows linear regressions for retention coefficients with HPLC retention time. With

reverse-phase HPLC, retention time is a direct proxy for molecular polarity, i.e. shorter retention times

395   indicate higher polarity and longer retention times indicate more nonpolar species. Both (−)HESI and

(+)HESI show significant negative correlation between retention and retention time and therefore

polarity; an F-test against the constant value model shows p-values of 0.00193 for (−)HESI and 1.44 ×

10^{-6} for (+)HESI. This indicates that nonpolar species are likely to be unretained and this appears to be

especially true for the previously discussed long chain species, such as $C_{14}H_{22}$ (190 *m/z*, 14.5 min, L3)

400   and $C_{15}H_{26}O$ (222 *m/z*, 14.6 min, L3) compounds. In Figure 7, a few compound classes separate distinctly

by polarity, particularly the CHOS and CHNO in (−)HESI as well as CHO and CHNO in (+)HESI. These

polarity differences in these classes may be the driving force in the difference of the freezing retention

between CHOS and CHNO in (−)HESI, but unlikely for CHO and CHNO in (+)HESI as CHO spans a much wider range of freezing retentions that cannot be explained solely by polarity.

405   The determined molecular weight (MW) shows little correlation linearly with freezing retention (as seen in Figure S2). In (−)HESI, the slope of the regression is weakly positive, suggesting larger compounds are more likely to be retained. This is likely related to lower vapor pressures associated with larger MW species in the negative mode. An F-test against the constant value model indicates that this correlation is not significant (p-value: 0.0857). However in (+)HESI, the slope of the regression is weakly

410   negative for MW which suggests the opposite. An F-test against the constant value model indicates that this correlation with MW is also not significant (p-value: 0.1440). This trend in the positive mode is likely driven more by polarity, as Figure 1.A also demonstrates that larger species in (+)HESI tend to have higher HPLC retention times and are therefore more nonpolar. The plot in Figure 7 further demonstrates this with a stronger negative correlation between the HPLC retention time and the freezing retention.

415
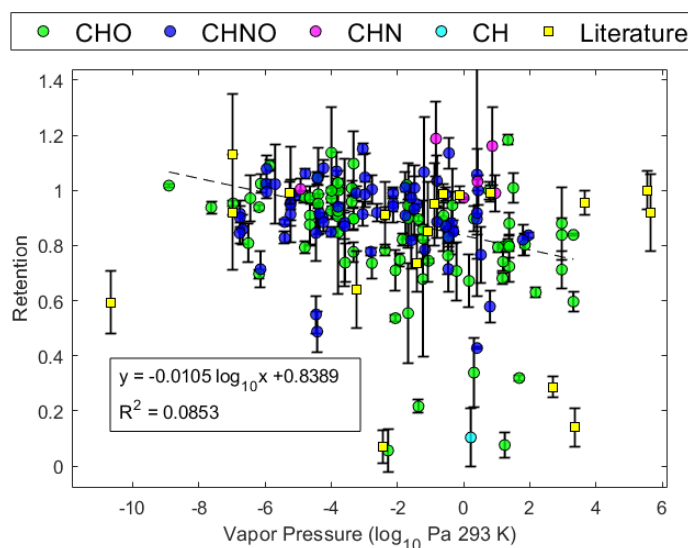
Figure 8. Retention Coefficient as a function of Estimated Vapor Pressure; Color denotes compositional class of the assigned compound: Green for CHO, blue for CHNO, magenta for CHN, cyan for CH, yellow squares for values taken from literature. Dashed line shows linear fit.

420

Further chemical property linear regressions with freezing retention could be made for the species with estimated chemical properties. The first plot, Figure 8, uses the measured retention coefficient to plot against calculated vapor pressure (VP). It demonstrates a significant negative correlation with VP; an F-test against the constant value model gives a p-value of 1.42×10^{-4}. It is relevant to note that the majority of species measured are considered semi-volatile (vapor pressure: 10^{-9} to 10 Pa; SVOC) with few low volatility (LVOC) and intermediate volatility organic compounds (IVOC) (Li et al., 2023; Manavi and Pandis, 2024). LVOC and IVOC are bias against in the sampling method as many LVOCs are highly oxygenated compounds which may be less sensitive compared to other compounds in UHPLC-Orbitrap MS (Wang et al., 2024) and most IVOCs are revolatilized during sampling (Bidleman et al., 2020). VP is also the property most associated with desorption effects, likely contributing to some of the negative trend seen in Figure 8. However, it is mostly associated with IVOC and less with SVOC so desorption alone is not likely to fully explain this correlation.
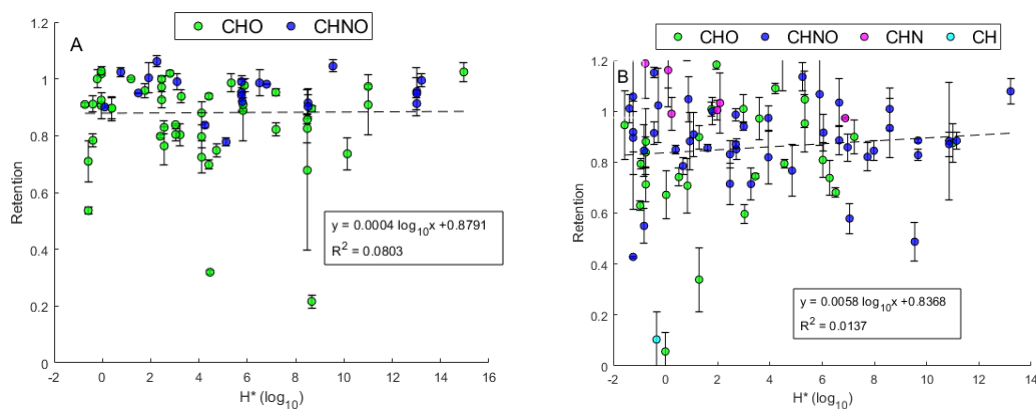
435   Figure 9. Effective Henry's Law Constant H* versus Retention Coefficient; (A) (−)HESI, (B) (+)HESI; Color denotes compositional class of the assigned compound: Green for CHO, blue for CHNO, magenta for CHN, cyan for CH. Dashed line shows linear fit.

    Demonstrated in Figure 9, freezing retention shows little or no dependency on H* under the

440   present experimental conditions. The linear regressions are not significant for neither (−)HESI or (+)HESI; with p-values of 0.9270 and 0.3530 respectively for the F-test against the constant value model. The very slight positive slope of the linear regression shows agreement with Stuart and Jacobson's (2003, 2004) observation that high H* species are more likely to be 100% retained but does not show sigmoidal behavior as modeled by Jost et al., 2017 (plotted for reference in Figure 10). This could be the result of

445   differing physical experimental parameters, such as larger droplet size (2 mm versus 20 micron). However, directly comparing the known literature values for retention coefficients with the observations made here does not immediately indicate the systems are incompatible or exclude the comparison.
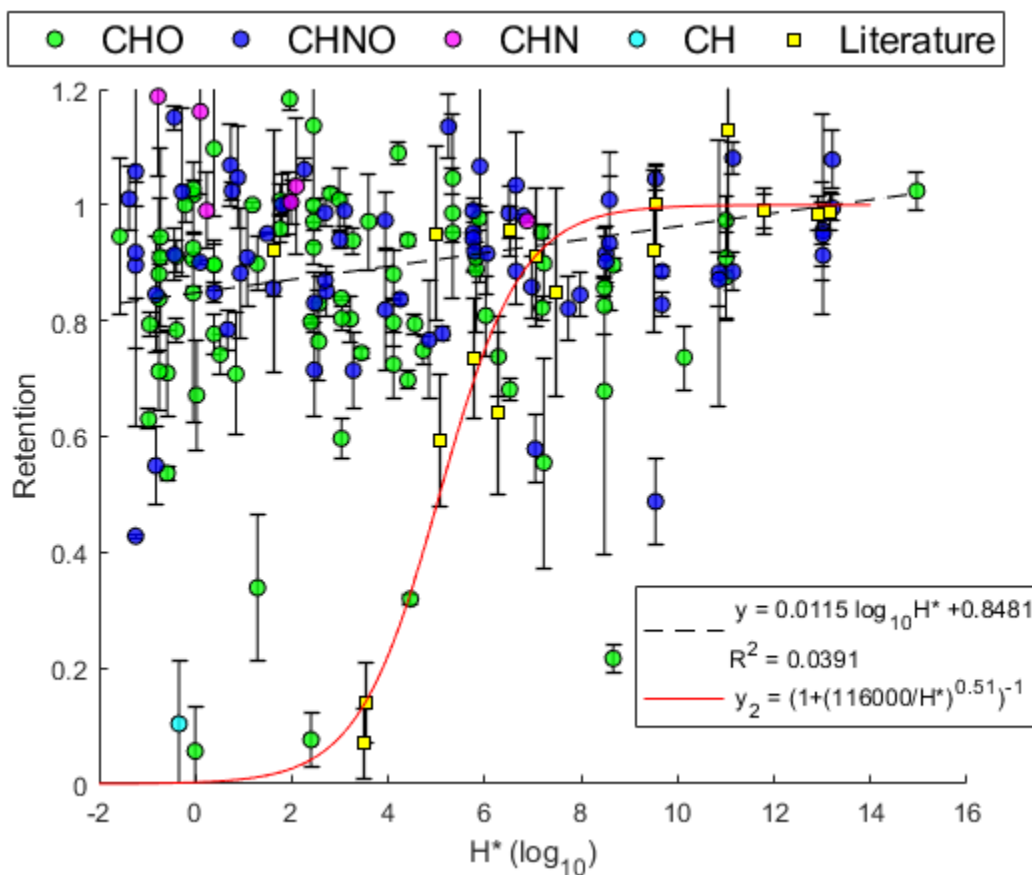
Figure 10. Effective Henry's Law Constant H* versus Retention Coefficient; Color denotes compositional class of the assigned compound: Green for CHO, blue for CHNO, magenta for CHN, cyan for CH; Yellow squares denote values taken from Borchers et al., (2024), Jost et al., (2017), and Von Blohn et al., (2011, 2013). Dashed line shows linear fit. Solid red line gives the parameterization by Jost et al., (2017).

Figure 10 compares the data presented in Figure 9 against the literature values presented by Borchers et al., (2024), Jost et al., (2017, and Von Blohn et al., (2011, 2013). This comparison does not appear incongruous, i.e. no discernible difference can be seen between wind tunnel experiments and these observations. While the measurements presented by Borchers et al., (2024), Jost et al., (2017), and Von Blohn et al., (2011, 2013) are physically dissimilar experiments to this study—i.e. wind tunnel experiments, small droplets of micrometer size, high ventilation conditions—their observations are congruent with this experiment. Additionally, there are chemical dissimilarities in these experiments, as

460   the present experiment is potentially influenced by activity differences from the extract solution's

complexity as opposed to the single or few component solutions used by the previously stated studies.

Further, the species studied in the current literature are mostly inorganics which are very different in

terms of solubility, polarity, and molecular size compared to organics studied here, i.e. generally more

soluble, more polar, and smaller. This could suggest that the organics measured here should have lower

465   retentions than the inorganics in the literature but that is not observed in the data. However, two of the

same nitrophenols studied by Borchers et al. (2024) are measured here: 4-nitrophenol and 2,4-

dinitrophenol. It's also likely that 2-nitrobenzoic acid and 4-nitrocatechol or similar analogues are

observed within the dataset since other nitroaromatics that cannot be structurally resolved are observed. 2-

nitrophenol is also potentially observed, however 2 and 4 nitrophenol are difficult to distinguish from

470   each other as structural isomers and 2-nitrophenol is not easily ionizable in this method. However, these

assignments cannot be confirmed without better structural information. The literature values include only

three species with $H^* < 10^4$ and two of them, pinanediol and formaldehyde, are excluded from the

parameterization presented by Borchers et al., (2024) as they were perceived as outliers. Without more

measurements of compounds with $H^* < 10^4$ under wind tunnel conditions, it is difficult to determine if the

475   nonsigmoidal behavior seen in this experiment is the result of different physical parameters—specifically

the lower surface-to-volume ratio—or if the sigmoidal behavior described by Borchers et al., (2024) and

Jost et al., (2017) is a fit of a limited dataset. Physical differences such as higher surface-to-volume ratio,

increased ventilation, or longer freezing times may result in lower retentions that may primarily affect

species with lower H^* as noted by Jost et al. (2017). Small riming droplets have freezing times in the tens

480   of milliseconds while the drops here take approximately 90 seconds to fully freeze. However, the ice shell

formation observed by Gautam et al. (2025) in Part 1 is quite fast, in the range of 5 ms. Specifically, these

differences either enhance heat and mass transfer which produces a shorter timescale for expulsion or

increases freezing time which allows for a wider range of expulsion timescales. Specifically, these

differences either enhance heat and mass transfer or provide a longer timescale for expulsion to occur.

485   Describing this in the framing of Stuart and Jacobson's (2003, 2004) model, species with larger H^* are

more likely to be unaffected by these differences as the gas-phase mass transport term and the interfacial mass transport term are still dominated by H* despite the decrease in spread droplet height and increase in thermal velocity such that the total expulsion time is still much longer than the freezing time. Evidence presented by Gautam et al., (2025) in part 1 of this publication series makes a compelling case for the dominance of physical parameters at these drop sizes. Critical to these experiments, Gautam et al., (2025) observed the formation of an ice shell, which inhibited any further expulsion of dissolved substances during freezing.

4 Conclusions

This study presents the measurement of the retention coefficients for real, complex WSOCs from urban particulate matter for direct drop freezing under raindrop size conditions. The overall distribution of the retention of WSOCs forms a real, nonnormal distribution up to 1. Looking at the individual compound classes of organics, the data shows that they may have different distributions of retention coefficients. Most negatively ionizable CHNO and CHOS compounds appear to be fully retained, indicating that nitroaromatics and organosulphates are favorable to be retained. Weak positive correlations between MW, polarity, and H* are seen with retention along with a negative correlation with vapor pressure (VP). No sigmoidal relationship with H* was observed. This is likely the result of the lower surface-to-volume ratio for this drop size and the ice shell formation observed by Gautam et al., (2025) in part 1 of this publication series. However, without further measurements of single component solutions for compounds with $H^* < 10^4$ under wind tunnel conditions, specifically for small cloud droplet sizes, it is difficult to determine if the nonsigmoidal behavior seen in this experiment is solely the result of physical parameters or if the sigmoidal behavior described by other studies is an overfit of a limited dataset.

The observed sulfides, lipids, aromatic hydrocarbons, and long chain compounds are among the

510 most unretained and incidentally the fewest species observed. These are also among the most nonpolar

species observed, which is presumably the dominant factor in that regard. CHO species show the highest

variability for their measured retentions, most likely related to the distributions of polarity and VPs

among the sugars, organic acids, and terpenoids seen here.

Aliphatic amines (AA) don't follow the trends associated with polarity and VP but are among the

515 most highly retained species. The explanation for this is possibly in its structural properties, which cannot

be easily determined using this analytical method. AA solubility in water is largely determined by the

dimension and structure of the alkyl substituents, such that AA with longer chains are less soluble than

AA with shorter chains and AA with branched substituents are less soluble than AA with linear groups

with the same number of carbons (Badocco et al., 2015). Polarity and hydrogen bonding are also known

520 contributors to AA solubility but this is not unique to AA. Indeed, solubility as a property relevant to

retention is applicable to all compounds, specifically in how aqueous solubility is related to H*. While

aqueous solubility is a piece of the typical bond method calculation to estimate H*, it does not necessarily

correlate with true H*. Further analysis on solubility as a factor for retention would be valuable but the

limitations on high confidence structural assignment in this method prevent its thorough investigation.

525 Structure assignment could also elucidate other retention relevant properties such as hydrogen bonding

potential or even acid/base effects. Hydrogen bonding potential may enhance retention along oxygen

functionalities such as among nitro and sulphate species. Hydrogen bonding alone, however, is unlikely to

fully explain the high retentions among nitro and sulphate species. Specifically, nitro species have weak

hydrogen bonding potential (Shugrue et al., 2016) and as a result is likely influenced mostly by the

530 increased polarity imparted by the nitro substituent or its dissociation.

The data suggests that functional groups containing sulfur or nitrogen generally increase a

species' ability to be retained. Overall, the high retentions of the nitro and sulfate species typically

anthropogenically related to NO_x and SO_2 chemistry, indicate that NO_x and SO_2 chemistry may enhance

the retention of these SOA species, reducing their likelihood of reaching the upper atmosphere. Further on

535   this, other studies have demonstrated that NOx participates in the reversible and irreversible uptake of

isoprene to aerosol liquid water and can further react with isoprene to produce a substantial number of

organonitrates (El-Sayed et al., 2018; Tsiligiannis et al., 2022). These findings may also indicate that this

NO_x chemistry on CHO species enhances their retention in hydrometeors, potentially by increasing its

polarity or solubility. Other UHRMS studies of rainwater have suggested similar explanations for nitrogen

540   uptake in hydrometeors and rainwater organic nitrogen's high bioavailability (Seymore et al., 2023).

Additionally, correlations with VP and polarity show that lower VP species and more polar species tend to

be retained. Atmospheric chemical processing generally tends to functionalize or oxidatively degrade

large nonpolar species into more water-soluble, less volatile species (John H. Seinfeld and Spyros N.

Pandis, 2019). Specifically, aqueous phase droplet chemistry is known to facilitate condensed phase SOA

545   formation from highly volatile species (McNeill, 2015). However, many freshly aged terpene products

increase in volatility or see only small decreases in VP with oxidation for their early generation products

(Bilde and Pandis, 2001; Kurtén et al., 2018; Wu et al., 2021). This indicates that many freshly oxidized

organics may have a lower potential to be retained than aged organics and may generally suggest that

freshly oxidized organics are more likely to reach the upper atmosphere than primary organics or aged

550   organics.

The use of UHPLC-HRMS has allowed for the study of ambient WSOC retention rather than

single component or limited mixture experiments from previous studies. While the influence on retention

due to activity differences resulting from matrix effects and solution complexity is still unknown, the

experiment in this paper demonstrates the viability of UHPLC-HRMS analysis for ambient WSOC and

555   shows the need for further complex mixture study regarding retention. Future studies on retention within

hydrometeors should include complex mixture analysis under the physical conditions most similar to the

atmosphere, i.e. wind tunnel experiments, smaller droplets, increased ventilation. As this experiment is a

first demonstration of retention within a complex mixture, the applicability of the conclusions here to

other locations or samplings with different aerosol compositions—thereby potentially different matrix effects—could be challenged. For example, black carbon particles suspended in a drop could strongly bind organic compounds, preventing their transition into the gas phase during freezing; certain surfactant species could change the surface accommodation, inhibiting exchange; or different amounts of inorganic ions could change the ionic strength of the aqueous phase, altering chemical potential. There is not enough evidence to assume these matrix effects are either negligible or the same elsewhere as in this experiment, but the assumption is not unreasonable. Rainwater tends to show negligible matrix effects for other properties and analyses (Pang et al., 2017; Sauret-Szczepanski et al., 2006). Average rainwater DOC is on the order of μM which could be assumed to be dilute enough for activity differences to be negligible compared to pure water solutions. However, these are still unsupported assumptions that are required for broad application of these conclusions. Additionally, broader application of these conclusions should consider the differences in relevant WSOC composition regarding seasons. This sample set is representative of winter aerosols, which show a high contribution from nitroaromatic compounds as well as a lower degree of oxidation and a lower proportion of organosulfates in comparison to the summer (Ma et al., 2022). It is also important to note that large-scale convective cloud formation where freezing retention is expected is not typical during the winter such as when the aerosols in the present study were sampled. Furthermore, in winter, frequent inversion and low mixing layer height tend to prevent surface emissions from being transported to higher altitudes and participate in ice cloud formation, so the compounds presented here may not be wholly representative of the most relevant species that participate in the retention process. Further studies would also be improved with more distinguishable tracers with known retentions and more sophisticated corrections for desorption. Further studies on single component solutions of species with $H^* < 10^4$ under atmospherically similar physical conditions would also allow for stronger conclusions from the comparison of the retentions measured in this study with other experiments performed under wind tunnel conditions.

The experiment presented here also cannot distinguish between species incorporated within ice crystal structure and those phase-separated but physically constrained to the hydrometeor, potentially between crystal grain boundaries or on the particle surface. That distinction is also not atmospherically relevant regarding the net transport of organics into the upper troposphere. While this method aims to demonstrate the retention for real WSOC, this method is still sample method biased against higher volatility species and likely features other sampling bias typical for HiVol filter based measurements such as filter extraction bias and solvation effects. These parameterizations of retention also present the distribution of retention coefficients for the variety of species present and not necessarily the mass distribution of species potentially present in the atmosphere. Corrections for species abundancy must first be made in order to apply the frequency distribution of the retention coefficients here to organic transport models.

Acknowledgements

Special thanks to Konstantin Dörholt for his initial work and experimentation in the Mainz Wind Tunnel with these samples.

This work was funded by the Deutsche Forschungsgemeinschaft (DFG, German Research Foundation) – TRR 301 – Project-ID 428312742.

This work was supported by the Max Planck Graduate Center with the Johannes Gutenberg University of Mainz (MPGC).

Author Contributions

JS, MG, MS, AT participated in designing the experiments; LZ provided the samples; JS, JM prepared the samples for experiments; MG performed the experiments; JS, JM, AV conducted the analytical

605   measurements; JS analyzed the data and wrote the manuscript draft; MG, MS, AT, JM, AV, TH reviewed

and edited the manuscript.

Competing Interests

The contact author has declared that none of the authors has any competing interests.

References

610

Andreae, M. O., Afchine, A., Albrecht, R., Holanda, B. A., Artaxo, P., Barbosa, H. M. J., Borrmann, S., Cecchini, M. A., Costa, A., Dollner, M., Fütterer, D., Järvinen, E., Jurkat, T., Klimach, T., Konemann, T., Knote, C., Krämer, M., Krisna, T., Machado, L. A. T., Mertes, S., Minikin, A., Pöhlker, C., Pöhlker, M. L., Pöschl, U., Rosenfeld, D., Sauer, D., Schlager, H., Schnaiter, M., Schneider, J., Schulz, C., Spanu, A.,
615   Sperling, V. B., Voigt, C., Walser, A., Wang, J., Weinzierl, B., Wendisch, M., and Ziereis, H.: Aerosol characteristics and particle production in the upper troposphere over the Amazon Basin, Atmos. Chem. Phys, 18, 921–961, https://doi.org/10.5194/acp-18-921-2018, 2018.

Andrés Casquero-Vera, J., Lyamani, H., Dada, L., Hakala, S., Paasonen, P., Román, R., Fraile, R., Petäjä, T., Olmo-Reyes, F. J., Alados-Arboledas, L., Andrés, J., and Vera, C.: New particle formation at urban and
620   high-altitude remote sites in the south-eastern Iberian Peninsula, Atmos. Chem. Phys, 20, 14253–14271, https://doi.org/10.5194/acp-20-14253-2020, 2020.

Badocco, D., Di Marco, V., Mondin, A., and Pastore, P.: Cyclic voltammetry as a new approach for the determination of solubility of aliphatic amines in water, J Chem Eng Data, 60, 895–901, https://doi.org/10.1021/je5009735, 2015.

625   Bardakov, R., Thornton, J. A., Riipinen, I., Krejci, R., and Ekman, A. M. L.: Transport and chemistry of isoprene and its oxidation products in deep convective clouds, Tellus B Chem Phys Meteorol, 73, 1–21, https://doi.org/10.1080/16000889.2021.1979856, 2021.

Bela, M. M., Barth, M. C., Toon, O. B., Fried, A., Ziegler, C., Cummings, K. A., Li, Y., Pickering, K. E., Homeyer, C. R., Morrison, H., Yang, Q., Mecikalski, R. M., Carey, L., Biggerstaff, M. I., Betten, D. P.,
630   and Alford, A. A.: Effects of Scavenging, Entrainment, and Aqueous Chemistry on Peroxides and Formaldehyde in Deep Convective Outflow Over the Central and Southeast United States, Journal of Geophysical Research: Atmospheres, 123, 7594–7614, https://doi.org/10.1029/2018JD028271, 2018.

Bidleman, T. F., Falconer, R. L., and Harner, T.: Particle/Gas Distribution of Semivolatile Organic Compounds: Field and Laboratory Experiments with Filtration Samplers, Gas and Particle Phase
635   Measurements of Atmospheric Organic Compounds, 39–71, https://doi.org/10.1201/9781003078340-4, 2020.

Bilde, M. and Pandis, S. N.: Evaporation rates and vapor pressures of individual aerosol species formed in the atmospheric oxidation of α- and β- pinene, Environ Sci Technol, 35, 3344–3349, https://doi.org/10.1021/es001946b, 2001.

640   Blair, S. L., MacMillan, A. C., Drozd, G. T., Goldstein, A. H., Chu, R. K., Paša-Tolić, L., Shaw, J. B., Tolić, N., Lin, P., Laskin, J., Laskin, A., and Nizkorodov, S. A.: Molecular Characterization of Organosulfur Compounds in Biodiesel and Diesel Fuel Secondary Organic Aerosol, Environ Sci Technol, 51, 119–127, https://doi.org/10.1021/ACS.EST.6B03304/SUPPL_FILE/ES6B03304_SI_002.XLSX, 2017.

645   Von Blohn, N., Diehl, K., Mitra, S. K., and Borrmann, S.: The retention of nitric acid, hydrochloric acid, and hydrogen peroxide Wind tunnel experiments on the retention of trace gases during riming: nitric acid, hydrochloric acid, and hydrogen peroxide The retention of nitric acid, hydrochloric acid, and hydrogen peroxide, Atmos. Chem. Phys. Discuss, 11, 17447–17472, https://doi.org/10.5194/acpd-11-17447-2011, 2011a.

650   Von Blohn, N., Diehl, K., Mitra, S. K., and Borrmann, S.: Wind tunnel experiments on the retention of trace gases during riming: Nitric acid, hydrochloric acid, and hydrogen peroxide, Atmos Chem Phys, 11, 11569–11579, https://doi.org/10.5194/ACP-11-11569-2011, 2011b.

Borchers, C., Seymore, J., Gautam, M., Dörholt, K., Müller, Y., Arndt, A., Gömmer, L., Ungeheuer, F., Szakáll, M., Borrmann, S., Theis, A., Vogel, A. L., and Hoffmann, T.: Retention of α-pinene oxidation
655   products and nitro-aromatic compounds during riming, https://doi.org/10.5194/egusphere-2024-1443, 2024.

Clarke, A. D., Varner, J. L., Eisele, F., Mauldin, R. L., Tanner, D., and Litchy, M.: Particle production in the remote marine atmosphere: Cloud outflow and subsidence during ACE 1, Journal of Geophysical Research Atmospheres, 103, 16397–16409, https://doi.org/10.1029/97JD02987, 1998.

660   Clarke, A. D., Eisele, F., Kapustin, V. N., Moore, K., Tanner, D., Mauldin, L., Litchy, M., Lienert, B., Carroll, M. A., and Albercook, G.: Nucleation in the equatorial free troposphere: Favorable environments during PEM-Tropics, Journal of Geophysical Research Atmospheres, 104, 5735–5744, https://doi.org/10.1029/98JD02303, 1999.

Compernolle, S. and Müller, J. F.: Henry's law constants of polyols, Atmos Chem Phys, 14, 12815–
665   12837, https://doi.org/10.5194/acp-14-12815-2014, 2014.

Diehl, K., Debertshäuser, M., Eppers, O., Schmithüsen, H., Mitra, S. K., and Borrmann, S.: Particle surface area dependence of mineral dust in immersion freezing mode: Investigations with freely suspended drops in an acoustic levitator and a vertical wind tunnel, Atmos Chem Phys, 14, 12343–12355, https://doi.org/10.5194/ACP-14-12343-2014, 2014.

670   Dusek, U., Frank, G. P., Hildebrandt, L., Curtius, J., Schneider, J., Walter, S., Chand, D., Drewnick, F., Hings, S., Jung, D., Borrmann, S., and Andreae, M. O.: Size matters more than chemistry for cloud-nucleating ability of aerosol particles, Science (1979), 312, 1375–1378, https://doi.org/10.1126/SCIENCE.1125261/SUPPL_FILE/DUSEK.SOM.PDF, 2006.

El-Sayed, M. M. H., Ortiz-Montalvo, D. L., and Hennigan, C. J.: The effects of isoprene and NOx on
675   secondary organic aerosols formed through reversible and irreversible uptake to aerosol water, Atmos Chem Phys, 18, 10.5194/acp-18-1171–2018, https://doi.org/10.5194/ACP-18-1171-2018, 2018.

Fofie, E. A., Donahue, N. M., and Asa-Awuku, A.: Cloud condensation nuclei activity and droplet formation of primary and secondary organic aerosol mixtures, Aerosol Science and Technology, 52, 242–251, https://doi.org/10.1080/02786826.2017.1392480/SUPPL_FILE/UAST_A_1392480_SM6542.PDF,
680   2018.

Hallquist, M., Wenger, J. C., Baltensperger, U., Rudich, Y., Simpson, D., Claeys, M., Dommen, J., Donahue, N. M., George, C., Goldstein, A. H., Hamilton, J. F., Herrmann, H., Hoffmann, T., Iinuma, Y., Jang, M., Jenkin, M. E., Jimenez, J. L., Kiendler-Scharr, A., Maenhaut, W., McFiggans, G., Mentel, T. F., Monod, A., Prévôt, A. S. H., Seinfeld, J. H., Surratt, J. D., Szmigielski, R., and Wildt, J.: The formation, properties and impact of secondary organic aerosol: Current and emerging issues, Atmos Chem Phys, 9, 5155–5236, https://doi.org/10.5194/acp-9-5155-2009, 2009.

Heitto, A., Wu, C., Aliaga, D., Blacutt, L., Chen, X., Gramlich, Y., Heikkinen, L., Huang, W., Krejci, R., Laj, P., Moreno, I., Sellegri, K., Velarde, F., Weinhold, K., Wiedensohler, A., Zha, Q., Bianchi, F., Andrade, M., Lehtinen, K. E. J., Mohr, C., and Yli-Juuti, T.: Analysis of atmospheric particle growth based on vapor concentrations measured at the high-altitude GAW station Chacaltaya in the Bolivian Andes, Atmos. Chem. Phys, 24, 1315–1328, https://doi.org/10.5194/acp-24-1315-2024, 2024.

Iinuma, Y., Müller, C., Berndt, T., Böge, O., Claeys, M., and Herrmann, H.: Evidence for the existence of organosulfates from β-pinene ozonolysis in ambient secondary organic aerosol, Environ Sci Technol, 41, 6678–6683, https://doi.org/10.1021/ES070938T/SUPPL_FILE/ES070938TSI20070723_080104.PDF, 2007.

Iribarne, J. V. and Pyshnov, T.: The effect of freezing on the composition of supercooled droplets—I. Retention of HCl, HNO3, NH3 and H2O2, Atmospheric Environment. Part A. General Topics, 24, 383–387, https://doi.org/10.1016/0960-1686(90)90118-7, 1990.

Isaacman-Vanwertz, G. and Aumont, B.: Impact of organic molecular structure on the estimation of atmospherically relevant physicochemical parameters, Atmos. Chem. Phys, 21, 6541–6563, https://doi.org/10.5194/acp-21-6541-2021, 2021.

John H. Seinfeld and Spyros N. Pandis: Atmospheric Chemistry and Physics: From Air Pollution to Climate Change, 3rd Edition, 1–1152 pp., 2019.

Jost, A., Szakáll, M., DIehl, K., Mitra, S. K., and Borrmann, S.: Chemistry of riming: The retention of organic and inorganic atmospheric trace constituents, Atmos Chem Phys, 17, 9717–9732, https://doi.org/10.5194/ACP-17-9717-2017, 2017.

Kaufmann, A. and Walker, S.: Comparison of linear intrascan and interscan dynamic ranges of Orbitrap and ion-mobility time-of-flight mass spectrometers, Rapid Communications in Mass Spectrometry, 31, 1915–1926, https://doi.org/10.1002/RCM.7981, 2017.

Kurtén, T., Hyttinen, N., Louise D'Ambro, E., Thornton, J., and Prisle, N. L.: Estimating the saturation vapor pressures of isoprene oxidation products C5H12O6 and C5H10O6 using COSMO-RS, Atmos Chem Phys, 18, 17589–17600, https://doi.org/10.5194/acp-18-17589-2018, 2018.

Lamb, D. and Verlinde, J.: Physics and Chemistry of Clouds, Cambridge University Press, 275–414 pp., https://doi.org/10.1017/CBO9780511976377, 2011.

Li, J., Gao, X., He, Y., Wang, L., Wang, Y., and Zeng, L.: Elevated emissions of melamine and its derivatives in the indoor environments of typical e-waste recycling facilities and adjacent communities and implications for human exposure, J Hazard Mater, 432, https://doi.org/10.1016/J.JHAZMAT.2022.128652, 2022.

Li, Y., Pöschl, U., and Shiraiwa, M.: Molecular corridors and parameterizations of volatility in the chemical evolution of organic aerosols, Atmos Chem Phys, 16, 3327–3344, https://doi.org/10.5194/ACP-16-3327-2016, 2016.

Li, Z., Hyttinen, N., Vainikka, M., Tikkasalo, O. P., Schobesberger, S., and Yli-Juuti, T.: Saturation vapor pressure characterization of selected low-volatility organic compounds using a residence time chamber, Atmos Chem Phys, 23, 6863–6877, https://doi.org/10.5194/ACP-23-6863-2023, 2023.

725 Liu, J., Zhang, F., Xu, W., Sun, Y., Chen, L., Li, S., Ren, J., Hu, B., Wu, H., and Zhang, R.: Hygroscopicity of Organic Aerosols Linked to Formation Mechanisms, Geophys Res Lett, 48, https://doi.org/10.1029/2020GL091683, 2021.

Liu, Z., Yim, S. H. L., Wang, C., and Lau, N. C.: The Impact of the Aerosol Direct Radiative Forcing on Deep Convection and Air Quality in the Pearl River Delta Region, Geophys Res Lett, 45, 4410–4418,
730 https://doi.org/10.1029/2018GL077517, 2018.

Ma, J., Ungeheuer, F., Zheng, F., Du, W., Wang, Y., Cai, J., Zhou, Y., Yan, C., Liu, Y., Kulmala, M., Daellenbach, K. R., and Vogel, A. L.: Nontarget Screening Exhibits a Seasonal Cycle of PM2.5Organic Aerosol Composition in Beijing, Environ Sci Technol, 56, 7017–7028, https://doi.org/10.1021/ACS.EST.1C06905/ASSET/IMAGES/LARGE/ES1C06905_0004.JPEG, 2022.

735 Manavi, S. E. I. and Pandis, S. N.: Contribution of intermediate-volatility organic compounds from on-road transport to secondary organic aerosol levels in Europe, Atmos Chem Phys, 24, 891–909, https://doi.org/10.5194/ACP-24-891-2024, 2024.

McNeill, V. F.: Aqueous organic chemistry in the atmosphere: Sources and chemical processing of organic aerosols, Environ Sci Technol, 49, 1237–1244, https://doi.org/10.1021/es5043707, 2015.

740 Nolan, J. P.: Univariate Stable Distributions, https://doi.org/10.1007/978-3-030-52915-4, 2020.

Pang, X., Lewis, A. C., and Shaw, M. D.: Analysis of biogenic carbonyl compounds in rainwater by stir bar sorptive extraction technique with chemical derivatization and gas chromatography-mass spectrometry, J Sep Sci, 40, 753–766, https://doi.org/10.1002/JSSC.201600561;JOURNAL:JOURNAL:15214168;CTYPE:STRING:JOURNAL
745 , 2017.

Price, D. J., Clark, C. H., Tang, X., Cocker, D. R., Purvis-Roberts, K. L., and Silva, P. J.: Proposed chemical mechanisms leading to secondary organic aerosol in the reactions of aliphatic amines with hydroxyl and nitrate radicals, Atmos Environ, 96, 135–144, https://doi.org/10.1016/J.ATMOSENV.2014.07.035, 2014.

750 Price, D. J., Kacarab, M., Cocker, D. R., Purvis-Roberts, K. L., and Silva, P. J.: Effects of temperature on the formation of secondary organic aerosol from amine precursors, Aerosol Science and Technology, 50, 1216–1226, https://doi.org/10.1080/02786826.2016.1236182, 2016.

Qi, L., Zhang, Z., Wang, X., Deng, F., Zhao, J., and Liu, H.: Molecular characterization of atmospheric particulate organosulfates in a port environment using ultrahigh resolution mass spectrometry:
755 Identification of traffic emissions, J Hazard Mater, 419, 126431, https://doi.org/10.1016/J.JHAZMAT.2021.126431, 2021.

Qian, K., Kumar, A., Patil, K., Bellmer, D., Wang, D., Yuan, W., and Huhnke, R. L.: Effects of Biomass Feedstocks and Gasification Conditions on the Physiochemical Properties of Char, Energies 2013, Vol. 6, Pages 3972-3986, 6, 3972–3986, https://doi.org/10.3390/EN6083972, 2013.

760 Riva, M., Chen, Y., Zhang, Y., Lei, Z., Olson, N., Chelmo, H. B., Narayan, S., Yee, L., Green, H., Cui, T., Zhang, Z., Baumann, K., Fort, M., Edgerton, E., Budisulistiorini, S., Rose, C., Ribeiro, I., Oliveira, R. e,

Santos, E. dos, Machado, C., Szopa, S., Zhao, Y., Alves, E., Sá, S. de, Hu, W., Knipping, E., Shaw, S., Junior, S. D., Souza, R. de, Palm, B., Jimenez, J., Glasius, M., Goldstein, A., Pye, H., Gold, A., Turpin, B., Vizuete, W., Martin, S., Thornton, J., Dutcher, C., Ault, A., and Surratt, J.: Rising Importance of Organosulfur Species for Aerosol Properties and Future Air Quality, https://doi.org/10.26434/CHEMRXIV.7597397.V1, 2019.

Sauret-Szczepanski, N., Mirabel, P., and Wortham, H.: Development of an SPME–GC–MS/MS method for the determination of pesticides in rainwater: Laboratory and field experiments, Environmental Pollution, 139, 133–142, https://doi.org/10.1016/J.ENVPOL.2005.04.024, 2006.

Saxena, P. and Hildemann, L. M.: Water-Soluble Organics in Atmospheric Particles: A Critical Review of the Literature and Application of Thermodynamics to Identify Candidate Compounds, J Atmos Chem, 24, 57–109, 1996.

Schollée, J. E., Schymanski, E. L., Stravs, M. A., Gulde, R., Thomaidis, N. S., and Hollender, J.: Similarity of High-Resolution Tandem Mass Spectrometry Spectra of Structurally Related Micropollutants and Transformation Products, J Am Soc Mass Spectrom, 28, 2692–2704, https://doi.org/10.1007/S13361-017-1797-6/ASSET/IMAGES/LARGE/JS8B05447_0005.JPEG, 2017.

Schymanski, E. L., Jeon, J., Gulde, R., Fenner, K., Ruff, M., Singer, H. P., and Hollender, J.: Identifying small molecules via high resolution mass spectrometry: Communicating confidence, Environ Sci Technol, 48, 2097–2098, https://doi.org/10.1021/ES5002105/ASSET/IMAGES/LARGE/ES-2014-002105_0001.JPEG, 2014.

Seymore, J., Felix, J. D., Abdulla, H., Bergmann, D., Campos, M. L. A. M., and Florêncio, J.: Pandemic-Related Anthropogenic Influences on the Dissolved Organic Matter Chemical Character in São Paulo State Wet Deposition by Ultrahigh-Resolution Mass Spectrometry, ACS Earth Space Chem, 7, 1929–1946, https://doi.org/10.1021/acsearthspacechem.3c00076, 2023.

Shugrue, C. R., Defrancisco, J. R., Metrano, A. J., Brink, B. D., Nomoto, R. S., and Linton, B. R.: Detection of weak hydrogen bonding to fluoro and nitro groups in solution using H/D exchange, Org Biomol Chem, 14, 2223–2227, https://doi.org/10.1039/C5OB02360B, 2016.

Snider, J. R., Montague, D. C., and Vali, G.: Hydrogen peroxide retention in rime ice, Journal of Geophysical Research: Atmospheres, 97, 7569–7578, https://doi.org/10.1029/92JD00237, 1992.

Stuart, A. L. and Jacobson, M. Z.: A timescale investigation of volatile chemical retention during hydrometeor freezing: Nonrime freezing and dry growth riming without spreading, Journal of Geophysical Research: Atmospheres, 108, https://doi.org/10.1029/2001JD001408, 2003.

Stuart, A. L. and Jacobson, M. Z.: Chemical retention during dry growth riming, Journal of Geophysical Research: Atmospheres, 109, https://doi.org/10.1029/2003JD004197, 2004.

Sun, H., Li, X., Zhu, C., Huo, Y., Zhu, Z., Wei, Y., Yao, L., Xiao, H., and Chen, J.: Molecular composition and optical property of humic-like substances (HULIS) in winter-time PM2.5 in the rural area of North China Plain, Atmos Environ, 252, 118316, https://doi.org/10.1016/j.atmosenv.2021.118316, 2021.

Surratt, J. D., Kroll, J. H., Kleindienst, T. E., Edney, E. O., Claeys, M., Sorooshian, A., Ng, N. L., Offenberg, J. H., Lewandowski, M., Jaoui, M., Flagan, R. C., and Seinfeld, J. H.: Evidence for organosulfates in secondary organic aerosol, Environ Sci Technol, 41, 517–527, https://doi.org/10.1021/ES062081Q/ASSET/IMAGES/LARGE/ES062081QF00006.JPEG, 2007.

Szakáll, M., Debertshäuser, M., Philipp Lackner, C., Mayer, A., Eppers, O., Diehl, K., Theis, A., Kumar Mitra, S., and Borrmann, S.: Comparative study on immersion freezing utilizing single-droplet levitation methods, Atmos Chem Phys, 21, 3289–3316, https://doi.org/10.5194/acp-21-3289-2021, 2021.

805   Taneda, S., Mori, Y., Kamata, K., Hayashi, H., Furuta, C., Li, C., Seki, K. I., Sakushima, A., Yoshino, S., Yamaki, K., Watanabe, G., Taya, K., and Suzuki, A. K.: Estrogenic and anti-androgenic activity of nitrophenols in diesel exhaust particles (DEP), Biol Pharm Bull, 27, 835–837, https://doi.org/10.1248/BPB.27.835, 2004.

Tsiligiannis, E., Wu, R., Lee, B. H., Salvador, C. M., Priestley, M., Carlsson, P. T. M., Kang, S., Novelli,
810   A., Vereecken, L., Fuchs, H., Mayhew, A. W., Hamilton, J. F., Edwards, P. M., Fry, J. L., Brownwood, B., Brown, S. S., Wild, R. J., Bannan, T. J., Coe, H., Allan, J., Surratt, J. D., Bacak, A., Artaxo, P., Percival, C., Guo, S., Hu, M., Wang, T., Mentel, T. F., Thornton, J. A., and Hallquist, M.: A Four Carbon Organonitrate as a Significant Product of Secondary Isoprene Chemistry, Geophys Res Lett, 49, e2021GL097366,
815   https://doi.org/10.1029/2021GL097366;WEBSITE:WEBSITE:AGUPUBS;JOURNAL:JOURNAL:19448 007;REQUESTEDJOURNAL:JOURNAL:19448007;WGROUP:STRING:PUBLICATION, 2022.

U. S. Environmental Protection Agency: Caprolactam - EPA Health Effects Notebook for Hazardous Air Pollutants, n.d.

US EPA: EPI Suite™-Estimation Program Interface | US EPA, https://www.epa.gov/tsca-screening-
820   tools/epi-suitetm-estimation-program-interface#citing.

Wang, K., Zhang, Y., Tong, H., Han, J., Fu, P., Huang, R. J., Zhang, H., and Hoffmann, T.: Molecular-Level Insights into the Relationship between Volatility of Organic Aerosol Constituents and PM2.5 Air Pollution Levels: A Study with Ultrahigh-Resolution Mass Spectrometry, Environ Sci Technol, 58, 7947–7957, https://doi.org/10.1021/acs.est.3c10662, 2024.

825   Weigel, R., Borrmann, S., Kazil, J., Minikin, A., Stohl, A., Wilson, J. C., Reeves, J. M., Kunkel, D., De Reus, M., Frey, W., Lovejoy, E. R., Volk, C. M., Viciani, S., D'amato, F., Schiller, C., Peter, T., Schlager, H., Cairo, F., Law, K. S., Shur, G. N., Belyaev, G. V, and Curtius, J.: Atmospheric Chemistry and Physics In situ observations of new particle formation in the tropical upper troposphere: the role of clouds and the nucleation mechanism, Atmos. Chem. Phys, 11, 9983–10010, https://doi.org/10.5194/acp-11-9983-2011,
830   2011.

Williamson, C. J., Kupc, A., Axisa, D., Bilsback, K. R., Bui, T. P., Campuzano-Jost, P., Dollner, M., Froyd, K. D., Hodshire, A. L., Jimenez, J. L., Kodros, J. K., Luo, G., Murphy, D. M., Nault, B. A., Ray, E. A., Weinzierl, B., Wilson, J. C., Yu, F., Yu, P., Pierce, J. R., and Brock, C. A.: A large source of cloud condensation nuclei from new particle formation in the tropics, Nature 2019 574:7778, 574, 399–403,
835   https://doi.org/10.1038/s41586-019-1638-9, 2019.

Wu, R., Vereecken, L., Tsiligiannis, E., Kang, S., Albrecht, S. R., Hantschke, L., Zhao, D., Novelli, A., Fuchs, H., Tillmann, R., Hohaus, T., Carlsson, P. T. M., Shenolikar, J., Bernard, F., Crowley, J. N., Fry, J. L., Brownwood, B., Thornton, J. A., Brown, S. S., Kiendler-Scharr, A., Wahner, A., Hallquist, M., and Mentel, T. F.: Molecular composition and volatility of multi-generation products formed from isoprene
840   oxidation by nitrate radical, Atmos Chem Phys, 21, 10799–10824, https://doi.org/10.5194/acp-21-10799-2021, 2021.

Xing, C., Wan, Y., Wang, Q., Kong, S., Huang, X., Ge, X., Xie, M., and Yu, H.: Molecular Characterization of Brown Carbon Chromophores in Atmospherically Relevant Samples and Their Gas-

Particle Distribution and Diurnal Variation in the Atmosphere, Journal of Geophysical Research: Atmospheres, 128, e2022JD038142, https://doi.org/10.1029/2022JD038142, 2023.

Yee, T. W.: Univariate Continuous Distributions, 343–370, https://doi.org/10.1007/978-1-4939-2818-7_12, 2015.

Zhang, Q., Anastasio, C., and Jimenez-Cruz, M.: Water-soluble organic nitrogen in atmospheric fine particles (PM2.5) from northern California, Journal of Geophysical Research: Atmospheres, 107, AAC 3-1, https://doi.org/10.1029/2001JD000870, 2002.

Zheng, G., Wang, Y., Wood, R., Jensen, M. P., Kuang, C., McCoy, I. L., Matthews, A., Mei, F., Tomlinson, J. M., Shilling, J. E., Zawadowicz, M. A., Crosbie, E., Moore, R., Ziemba, L., Andreae, M. O., and Wang, J.: New particle formation in the remote marine boundary layer, Nature Communications 2021 12:1, 12, 1–10, https://doi.org/10.1038/s41467-020-20773-1, 2021.

845

850

855